

Energy dependence of angular distributions in the nonanalog pion double-charge-exchange reaction $^{16}\text{O}(\pi^+, \pi^-)^{16}\text{Ne}(\text{g.s.})$

R. Gilman, H. T. Fortune, Kalvir S. Dhuga, and Peter H. Kutt
University of Pennsylvania, Philadelphia, Pennsylvania 19104

L. C. Bland, Rex R. Kiziah, C. Fred Moore, and Peter A. Seidl
University of Texas at Austin, Austin, Texas 78712

C. L. Morris
Los Alamos National Laboratory, Los Alamos, New Mexico 87545

W. B. Cottingham
New Mexico State University, Las Cruces, New Mexico 88003
(Received 5 March 1984)

Previous measurements have shown that pion double-charge-exchange angular distributions between nonanalog $J^\pi = 0^+$ states at $T_\pi = 164$ MeV are consistent with simple diffractive scattering, whereas angular distributions between analog $J^\pi = 0^+$ states at $T_\pi = 164$ MeV are not. We present measurements of angular distributions for the nonanalog reaction $^{16}\text{O}(\pi^+, \pi^-)^{16}\text{Ne}(\text{g.s.})$ at two additional energies and compare the energy dependence with that expected for diffractive scattering.

All reported measurements of $J^\pi = 0^+$ to 0^+ , (g.s.) to (g.s.) pion double-charge-exchange (DCX) transitions in which the initial and residual nuclear states are not analogs show a consistent set of characteristics. Those characteristics, summarized for $T = 0$ to $T = 2$ transitions in Ref. 1, have been confirmed in more recent measurements.^{2,3} Of those characteristics, the most pertinent to this Rapid Communication is that angular distributions at $T_\pi = 164$ MeV are all consistent with a diffractive scattering (strong absorption) process. In contrast, all measured analog DCX angular distributions⁴⁻⁶ are inconsistent with simple diffractive scattering (but can be explained with a more complex model^{7,8}). Four nonanalog angular distributions at $T_\pi = 164$ MeV have been reported: $^{16}\text{O}(\pi^+, \pi^-)^{16}\text{Ne}(\text{g.s.})$,⁹ $^{12}\text{C}(\pi^+, \pi^-)^{12}\text{O}(\text{g.s.})$,¹ $^{40}\text{Ca}(\pi^+, \pi^-)^{40}\text{Ti}(\text{g.s.})$,¹ and $^{18}\text{O}(\pi^-, \pi^+)^{18}\text{C}(\text{g.s.})$.³ We have measured angular distributions for $^{16}\text{O}(\pi^+, \pi^-)^{16}\text{Ne}(\text{g.s.})$ at two additional energies, $T_\pi = 120$ and 200 MeV, to investigate the energy dependence of nonanalog DCX angular distributions.

There is no general theory for nonanalog transitions. The work of Liu⁷ is not restricted to analog transitions, but calculations of nonanalog transitions require final-state wave functions for exotic nuclei, e.g., $^{16}\text{Ne}(\text{g.s.})$, and have not been done. A calculation¹⁰ of the ratio of cross sections for $^{16,18}\text{O}(\pi^+, \pi^-)^{16,18}\text{Ne}(\text{g.s.})$ at $T_\pi = 140$ MeV agrees roughly with the measured ratio (calculated to be ~ 3 , but measured recently¹¹ to be 4.9 ± 1.6 at $\theta = 5^\circ$), but fails to account for the rapid variation of the ratio with energy¹¹ or the difference in shape of angular distributions for the two reactions at $T_\pi = 164$ MeV.⁹ It should be noted that both of the above models assume that DCX on $T = 0$ targets proceeds via a sequential charge transfer (SCT) mechanism [see Fig. 1(a)], and that both are sensitive to nuclear structure effects (core excitation). The work of Johnson and Siciliano,⁸ also based on the diagram in Fig. 1(a), explicitly assumes isospin invariance; only analog transitions are calculated. It has been speculated,¹² as transitions between analog and nonanalog states have different energy dependence,

angle dependence at $T_\pi = 164$ MeV, and target mass dependence (see Refs. 1 and 6), that the dominant reaction mechanisms are different in the two cases. In particular, it was suggested¹² that diagram (c) of Fig. 1 is responsible for nonanalog DCX. Calculations of DCX from all the non-SCT mechanisms [diagrams (b), (c), and (d)] of Fig. 1 are underway by Johnson *et al.*¹³

Data were obtained with the DCX modifications⁵ to the Energetic Pion Channel and Spectrometer (EPICS) at the Clinton P. Anderson Meson Physics Facility (LAMPF). Three ^{16}O targets were used. All targets were water (of natural isotopic purity) frozen in a copper frame. The areal densities, types of entrance and exit windows, and data points obtained with each target are specified in Table I. The "two-gram" target was used initially for enhanced count rates. It was replaced by the "one-gram" target to improve energy resolution. The "Mylar" target was used to reduce background in the spectra that arose from continuum DCX on the copper windows.

Background became an important problem at larger angles, at which the ^{16}O cross sections are small. The background from the aluminized Mylar was much smaller than that from the copper for two reasons. First, the number of copper atoms was much larger than the number of aluminum atoms (the ratio was ~ 100). Second, Mylar consists of hydrogen (on which there is no DCX), oxygen (a negligibly small amount compared with the full target), and carbon (99% ^{12}C , which has a more negative DCX Q value than ^{16}O). There was, in addition, background from continuum DCX on ^{18}O in the natural isotopic purity water target. Background problems from the ^{18}O and copper windows were of similar size, as (with the one-gram target) the ratio of copper atoms to ^{18}O atoms was ~ 4 . The DCX Q values (in MeV) are -28.38 for ^{16}O , -7.85 for ^{63}Cu , -3.59 for ^{65}Cu , -16.38 for ^{27}Al , -31.96 for ^{12}C , and -5.08 for ^{18}O .

Absolute normalization factors were determined by measuring $^1\text{H}(\pi^+, \pi^+)^1\text{H}$ yields on a CH_2 target at 40° (laboratory) at all energies at which data were taken. The

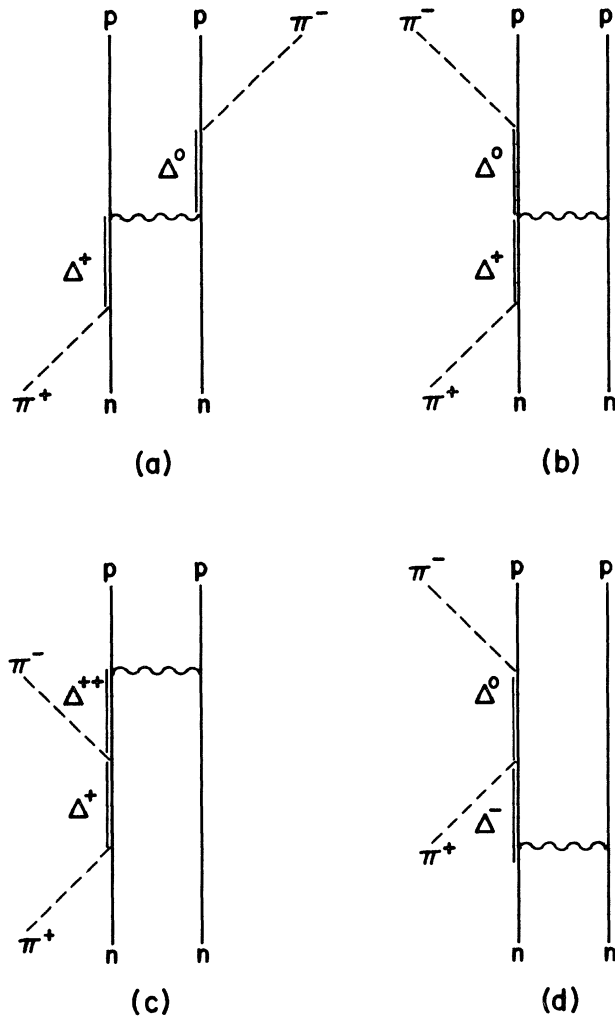


FIG. 1. diagrams for pion DCX. Diagram (a) is the usual sequential charge transfer mechanism. It has been speculated (Ref. 12) that diagram (c) is the dominant mechanism of nonanalog DCX. Work is in progress (Ref. 13) to evaluate diagrams (b), (c), and (d) for nonanalog transitions.

ratio of hydrogen cross section, calculated from the phase shifts of Rowe, Salomon, and Landau,¹⁴ to yield is a normalization factor that accounts for the product of the solid angle of the spectrometer and the number of pions in the incident beam. The absolute normalization factors are believed accurate to $\sim 10\%$. This uncertainty is the sum of

several errors, each of $\sim 3\%$, that include statistical errors on measuring the yield of ${}^1\text{H}(\pi^+, \pi^+){}^1\text{H}$, uncertainties in monitoring the primary beam flux, and uncertainties in calculating various correction factors such as the pion survival fraction and detection efficiencies. Typically, repeated normalization runs agree within statistical errors. Three normalization runs at $T_\pi = 200$ MeV, including one at 43° , yielded the same normalization factor, within statistical errors. A weighted average of these factors was used to normalize the $T_\pi = 200$ MeV data. Four runs at $T_\pi = 120$ MeV, including one at 43° , however, did not agree as well. The normalization factors were divided into two pairs. Agreement within each pair was better than 3% , but the pairs differed by $\sim 13\%$. Although there is evidence of some differences between the two pairs of runs, there is no evidence that any of the measurements is wrong. Thus we have used a weighted average of the four runs to normalize the $T_\pi = 120$ MeV data.

As a check on physically measured target thicknesses, ${}^1\text{H}(\pi^+, \pi^+){}^1\text{H}$ yields were measured with two of the three targets. This measurement gives a ratio of hydrogen in the water targets to hydrogen in the CH_2 target. Since the CH_2 target areal density is accurately known (73.69 mg/cm² CH_2), a water target areal density can be calculated. The result for the two-gram target, 1.66 ± 0.07 g/cm² of ${}^{16}\text{O}$, is slightly lower than the physically measured value of 1.78 g/cm² given in Table I. It is believed that this slight difference arises from the high count rates at which the H_2O measurement was made ($\sim 0.5 \times 10^6/\text{sec}$). The result for the Mylar target, 0.755 ± 0.021 g/cm² of ${}^{16}\text{O}$, agrees well with the value in Table I.

As a check on angle-dependent effects, hydrogen yields were measured as a function of angle. For part of the experiment, a wedge was inserted between the scattering chamber and the bellows that couples the scattering chamber to the pion beam channel to allow measurements at slightly larger scattering angles. Ratios of hydrogen cross sections, calculated as above, to yields measured from 15° to 40° without the wedge, and from 30° to 45° with the wedge, were constant within error bars ($\sim 3\%$).

As a final check on our overall normalization, a four-point excitation function at $\theta_{\text{lab}} = 5^\circ$ was measured. Figure 2 shows the overlap between this work and previous measurements.^{9,11} The repeated point at 164 MeV agrees well with the previous measurement, whereas the new point at 210 MeV is higher than the previously measured value,¹¹ but not inconsistent given the statistical uncertainties. The two new points at $T_\pi = 120$ and 200 MeV fit smoothly into the excitation function.

TABLE I. Target properties.

Target (Label)	$x\rho({}^{16}\text{O})$ (g/cm ²)	Window foils	Data obtained	
			T_π (MeV)	θ (deg)
"Two-gram"	1.78	Copper	120	5,15,25,35,45
			164	5
			200	15
			210	5
"One-gram"	0.75	Copper	200	5,15,25,35,43
"Mylar"	0.75	Aluminized Mylar	120	40
			200	5,20,30,43

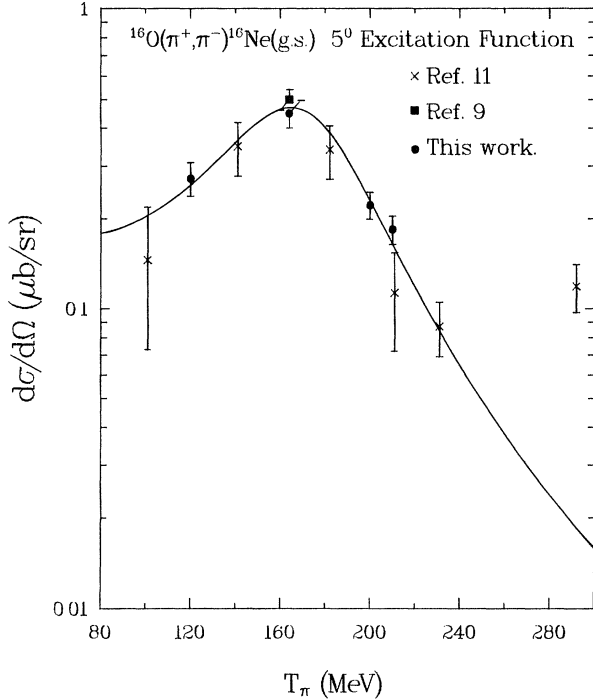


FIG. 2. Excitation function at $\theta = 5^\circ$ (laboratory) for $^{16}\text{O}(\pi^+, \pi^-)^{16}\text{Ne}(\text{g.s.})$. The curve is a Breit Wigner fit to all the data (except the 292-MeV point) with parameters $T_{\text{res}} = 171$ MeV and width $\Gamma = 75$ MeV.

Angular distributions for $5^\circ \leq \theta_{\text{lab}} \leq 45^\circ$ ($5^\circ \leq \theta_{\text{lab}} \leq 43^\circ$) were measured at $T_\pi = 120$ (200 MeV). These angular distributions, along with a previous measurement⁹ at $T_\pi = 164$ MeV, are plotted versus the momentum transfer in Fig. 3. It is apparent that the minima occur at about the same momentum transfer at all energies, as is expected for simple diffractive scattering. The curves displayed are damped Bessel functions, calculated from $\sigma = NJ_0^2(qR)e^{-qd}$, with parameters that best fit the data. These parameters are given in Table II. Both the radius R and damping factor d are, within uncertainties, independent of energy. Thus, except for an overall scale factor, the angular distributions are essentially the same at all energies. The large uncertainties in d merely reflect the insensitivity of the fit to the value of d . However, these uncertainties in d contribute insignificantly to the uncertainties in R .

It should be noted that the radius we have extracted, $R \sim 3.4$ fm, is a reasonable value for the strong-absorption radius of ^{16}O . The one-tenth (two-tenths) density point of ^{16}O , calculated from the parametrizations of Ref. 15, is about 3.7 fm (3.3 fm). Of course, as the energy is varied

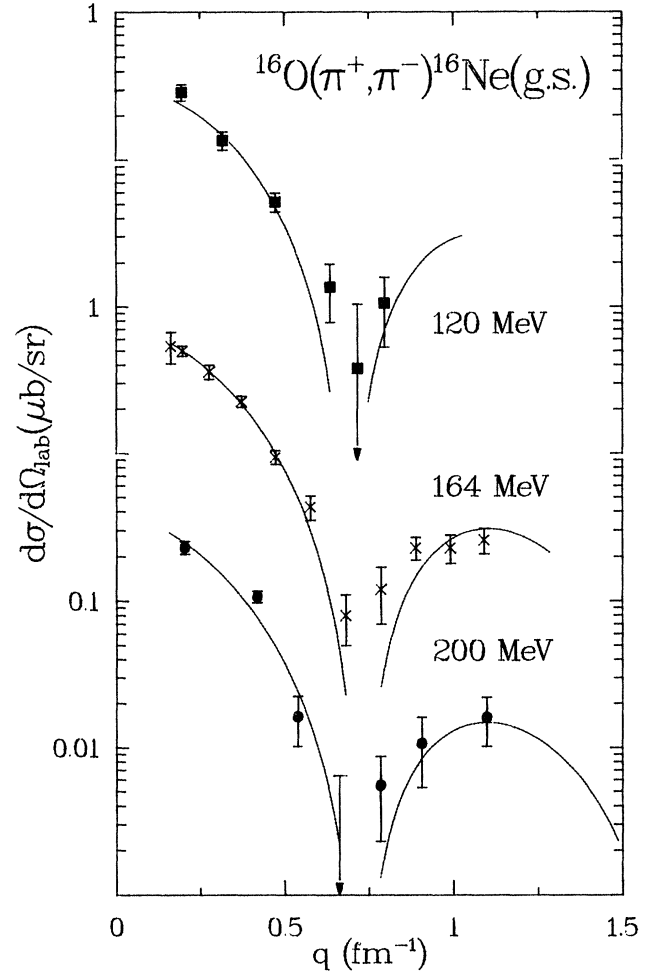


FIG. 3. Angular distributions for $^{16}\text{O}(\pi^+, \pi^-)^{16}\text{Ne}(\text{g.s.})$ at three energies. The angular distribution at $T_\pi = 164$ MeV is from Ref. 9. The curves displayed are the damped Bessel functions, calculated from $\sigma = NJ_0^2(qR)e^{-qd}$, that best fit the data. All curves extend over the same angular range, $0^\circ \leq \theta \leq 60^\circ$. Fit parameters are given in Table II.

across the $\Delta_{3,3}$ resonance, the validity of the strong-absorption assumption varies, and the effective radius is expected to be a function of energy. Estimates of the strong-absorption radius from the values of σ_{tot} in Ref. 16 indicate that this radius is nearly constant between $T_\pi = 120$ and 164 MeV, and is 5% smaller at 200 MeV. Our measurements are not sensitive to an effect of that magnitude.

In Table III we list, for the three bombarding energies, the 5° cross section, the normalization factor from the

TABLE II. Best fit parameters [$\sigma(q) = NJ_0^2(qR)e^{-qd}$] for ^{16}O angular distributions.

T_π (MeV)	χ^2	N ($\mu\text{b}/\text{sr}$)	R (fm)	d (fm)
120	3.17	0.334	3.48 ± 0.23	0.51 ± 1.19
164	2.31	0.810	3.30 ± 0.16	1.28 ± 0.44
200	4.30	0.411	3.31 ± 0.19	1.32 ± 0.39

TABLE III. Energy dependence of the cross sections.

T_π (MeV)	$\sigma(5^\circ)$ (nb/sr)	N (nb/sr)	$\sigma_{\text{tot}}(0^\circ-50^\circ)$ (nb)
120	273 ± 35	334	92
164	449 ± 49	810	140
200	222 ± 23	411	60

angular-distribution fits, and the angle-integrated ($\theta = 0^\circ-50^\circ$) cross section. The three quantities all exhibit the same trend—a peak at 164 MeV with a rapid falloff on either side. With a damping factor d as large as 1.0 fm, if the angular distributions are of the form $\sigma = NJ_0^2(qR)e^{-qd}$, then the $0^\circ-50^\circ$ integrated cross section is more than half of that for $0^\circ-180^\circ$. Hence it is clear that the peak in the excitation function is not an artifact of an anomalous 5° behavior. The angular distribution as a whole goes up and down rapidly with increasing bombarding energy.

In conclusion, angular distributions for the

$^{16}\text{O}(\pi^+, \pi^-)^{16}\text{Ne}(\text{g.s.})$ reaction are functions of the momentum transfer q , which are independent of energy (except for an overall scale factor) within the accuracy of our measurement. This energy dependence is consistent with strong-absorption scattering, in sharp contrast to the observed behavior of angular distributions for analog DCX transitions,⁶ for which the minima at $T_\pi = 164$ MeV (292 MeV) are at $qR \sim 1.7$ (3.5). Minima for $^{16}\text{O}(\pi^+, \pi^-)^{16}\text{Ne}(\text{g.s.})$ are at $qR = 2.4$ at all measured energies. Any correct theory of nonanalog DCX must predict diffractive angular distributions at all energies, forward angle excitation functions that peak near $T_\pi = 160$ MeV, and a smooth $A^{-4/3}$ mass dependence for $T=0$ to $T=2$ transitions.

We thank Andrew Harvier of the MP-10 technical staff for preparation of the ice targets, and acknowledge several discussions with Mikkel Johnson. This work was supported in part by the U.S. Department of Energy, The Robert A. Welch Foundation, the National Science Foundation, and the Natural Sciences and Engineering Research Council of Canada.

¹L. C. Bland, R. Gilman, M. Carchidi, K. Dhuga, Christopher L. Morris, H. T. Fortune, S. J. Greene, Peter A. Seidl, and C. Fred Moore, Phys. Lett. **128B**, 157 (1983).

²Peter A. Seidl, Rex R. Kiziah, Mark K. Brown, C. Fred Moore, C. L. Morris, Helmut Baer, Steven J. Greene, G. R. Burlinson, W. B. Cottingham, L. C. Bland, R. Gilman, and H. T. Fortune, Phys. Rev. Lett. **50**, 1106 (1983).

³R. Gilman, H. T. Fortune, L. C. Bland, Rex R. Kiziah, C. Fred Moore, Peter A. Seidl, C. L. Morris, and W. B. Cottingham (submitted to Phys. Rev. C).

⁴Kamal K. Seth, S. Iversen, H. Nann, M. Kaletka, J. Hird, and H. A. Thiessen, Phys. Rev. Lett. **43**, 1574 (1979); **45**, 147 (1980).

⁵S. J. Greene, W. J. Braithwaite, D. B. Holtkamp, W. B. Cottingham, C. Fred Moore, C. L. Morris, H. A. Thiessen, G. R. Burlinson, and G. S. Blanpied, Phys. Lett. **88B**, 62 (1979).

⁶Peter A. Seidl, Rex R. Kiziah, Mark K. Brown, C. Fred Moore, C. L. Morris, Helmut Baer, Steven J. Greene, G. R. Burlinson, W. B. Cottingham, L. C. Bland, R. Gilman, and H. T. Fortune (submitted to Phys. Rev. C).

⁷L. C. Liu, Phys. Rev. C **27**, 1611 (1983).

⁸Mikkel B. Johnson and E. R. Siciliano, Phys. Rev. C **27**, 730 (1983); **27**, 1647 (1983).

⁹S. J. Greene, W. B. Cottingham, G. R. Burlinson, L. C. Bland, R. Gilman, H. T. Fortune, C. L. Morris, D. B. Holtkamp, C. Fred Moore, Phys. Rev. C **27**, 2375 (1983).

¹⁰T.-S. H. Lee, D. Kurath, and B. Zeidman, Phys. Rev. Lett. **39**, 1307 (1977).

¹¹S. J. Greene, W. J. Braithwaite, D. B. Holtkamp, W. B. Cottingham, C. Fred Moore, G. S. Blanpied, A. T. Viescas, G. H. Daw, C. L. Morris, and H. A. Thiessen, Phys. Rev. C **25**, 927 (1982).

¹²C. L. Morris, H. T. Fortune, L. C. Bland, R. Gilman, S. J. Greene, W. B. Cottingham, D. B. Holtkamp, G. R. Burlinson, and C. Fred Moore, Phys. Rev. C **25**, 3218 (1982).

¹³Mikkel B. Johnson *et al.* (unpublished).

¹⁴G. Rowe, M. Salomon, and Rubin H. Landau, Phys. Rev. C **18**, 584 (1978).

¹⁵C. W. de Jager, H. de Vries, and C. de Vries, At. Data Nucl. Data Tables **14**, 479 (1974).

¹⁶J. P. Albanese, J. Arvieux, J. Bolger, E. Boschitz, C. H. Q. Ingram, J. Jansen, and J. Zichy, Nucl. Phys. **A350**, 301 (1980).